INSTRUMENTATION

Quantitative Multi-Detector Emission Computerized Tomography Using Iterative Attenuation Compensation

Stephen C. Moore, Jacques A. Brunelle,* and Carl-Martin Kirsch†

Harvard Medical School and Brigham and Women's Hospital, Boston, Massachusetts

An iterative procedure to correct for attenuation has been developed for a multi-detector, single-photon emission tomographic scanner. The difference between measured and estimated data projections is used at each iteration to form an error image which is used, in turn, to correct the image. A damping factor that minimizes χ^2 is applied after each iteration to speed convergence. Several phantoms of different size, with various concentration distributions, have been used to compare this method with a first-order multiplicative attenuation correction used previously with this scanner. The first-order correction is inadequate for most of the phantoms studied, whereas relative and absolute quantitative capability is demonstrated for the iterative attenuation correction. The reconstructed average number of counts per pixel is a linear function of activity concentration up to ~5 μCi/ml for all regions of uniform activity whose size is ≥5 cm. The importance of using an accurate attenuation distribution with this method is demonstrated with a torso-like phantom.

J Nucl Med 23: 706–714, 1982

In a recent paper, Kirsch et al. (*1*) evaluated the physical imaging characteristics of a multi-detector, single-photon emission computed tomographic (ECT) scanner.‡ Although this whole-body instrument exhibits the useful properties of high single-slice sensitivity and a spatially invariant line response function, its major drawback was reported to be a nonuniform spatial response in the ratio of source-to-background activity concentrations, when measured in objects of extended activity distributions.

The most serious problem affecting the ability of single-photon emission tomography instruments to provide accurate, quantitative measurements of radionuclide concentrations is the difficulty of correcting reconstructed images for the usually nonuniform attenuation of emitted radiation. The usual methods for inverting the Radon integral equation to obtain an image from measured projection data do not apply when the measurement process exponentially couples the source distribution to the distribution of attenuating material. For photon energies most commonly used in nuclear medical studies (~140 keV), the effect of attenuation is nonlinear. For this reason, the first-order multiplicative corrections (*1–5*) to the raw data before filtering, or to the reconstructed image, do not always work for the case of spatially extended source distributions of varying concentrations.

Several compensation methods have been proposed. Those that attempt to invert the *attenuated* Radon transform analytically (*6–9*) are elegant and fast, but they rely on the approximation that the attenuating material be convex in shape and of uniform attenuation.

Received Oct. 14, 1981; revision accepted March 22, 1982.

For reprints contact: Stephen C. Moore, Ph.D., Dept of Radiology, Div. of Physics and Engineering, Harvard Medical School, 44 Binney St., Boston, MA 02115.

* Present address: Ortho Instruments, 410 University Ave., Westwood, MA 02090.

† Present address: Abt. Nuklearmedizin, Klinikum Grosshadern, Universität München, 8000 München 70, FRG.

Iterative methods (*5,10,11*), which attempt to match real projection data with projections estimated from a known or assumed attenuation distribution, are generally slower but potentially more accurate than the analytic methods.

An iterative correction has been developed for the multi-detector, single-photon emission tomographic scanner (*1,12*). The instrument's operation is briefly described in the next section. This is followed by a description of the correction method. Results of tests of the method are presented in the fourth section, followed by a comparative discussion in the last section.

THE MULTI-DETECTOR SCANNER

The instrument contains ten identical detectors in a circular configuration around the patient. Each detector uses a 20 cm × 12.5 × 2.5 cm NaI(Tl) detector equipped with a focussed collimator, and scans the field of view tangentially, with its focal point moving through the object. After a line is scanned, one detector is moved radially outward while its opposing detector is moved inward the same distance. The next tangential line is then scanned. All ten detectors scan half the total field of view. The entire ring of detectors is then rotated 18° (half the angular separation between detectors) and the same scan pattern is repeated, resulting in 20 two-dimensional projections at 18° intervals for the reconstruction of one transverse slice.

The reconstruction used previously (*1,12*) contained a first-order correction for attenuation. A multiplicative correction was applied to each two-dimensional raw-data projection. The correction grid calculation assumed a circular object of uniform attenuation, centered within the gantry. Each correction factor was simply an exponential function of the distance from the grid point to the object boundary along a line perpendicular to the tangential scan direction of the detectors.

Each tangential scan row of data was then filtered using the one-dimensional convolution function in Table 1. This convolver was an empirically determined medium-pass (ramp with roll-off) filter.[§] Each convolved data point in each 128 × 22 projection was then added to the 128 × 128 reconstruction grid at its focal-point position using bilinear interpolation to the four nearest neighbor points. It has not been theoretically proven that this reconstruction successfully inverts the Radon integral equation for this geometry to obtain an image from the measured projections. However, a plausible heuristic explanation has been described by Stoddart and Stoddart (*12*).

Kirsch et al. (*1*), in addition to reporting inaccuracies in the measurement of source-to-background activity ratios, also examined the noise properties of the machine. They concluded that the reconstruction amplifies the random noise to a level ~3.2 times what would be expected for a rotating gamma camera of the same spatial resolution recording 144 projections. This was attributed to the limited angular sampling of the scanning, multi-detector system. It encouraged us to try an iterative technique to correct for attenuation, instead of a direct analytic inversion of the attenuated Radon transform. Gullberg and Budinger (*8*) showed that direct analytic approaches can produce serious aliasing artifacts for the case of limited angular sampling, whereas iterative techniques generally converge to the smoothest possible fit to the measured projection data, thus minimizing noise. In addition, we could accommodate nonuniform attenuation distributions in the reconstruction with little difficulty.

Using a first-order precorrection for a smaller scanning multi-detector system that was designed for brain imaging (*13*), Flower et al. (*14*) also reported errors in the measurement of radionuclide concentration. The iterative technique described here for the whole-body scanner could easily be applied to the brain machine.

THEORY

Several different iterative approaches have been suggested. What they all have in common is an accurate means of estimating the projection data that would be obtained by scanning a hypothetical radionuclide activity distribution contained within a measured or assumed distribution of attenuating material. Thus, the first step is to obtain an estimated, or starting, image for the iterative process. This is often accomplished by a convolution-back-projection reconstruction, perhaps with a first-order, multiplicative correction for attenuation. Data projections are then estimated for this starting image by taking into account the attenuation along each projection ray. (These factors are precalculated from the measured or assumed attenuation distribution.) The difference between these estimated projections and the real data projections is then used to correct the starting image. The manner in which the difference, or error, projections are used to change the reconstructed image at each iteration is the principal difference between the various iterative techniques. Most of them try to find a correction method that will minimize χ^2 on the following iteration. (χ^2 is the sum of the squares of each point in the difference projections divided by the square of the measurement error at that point.) An iterative least-squares technique (ILST) with attenuation factors used as weights was studied by Budinger and Gullberg (*5*). This type of iterative approach was first described in the context of tomographic reconstruction by Goitein (*15*). ILST uses information from all projections to compute the whole correction matrix at each iteration.

More recently, Huesman et al. (*16*) described a similar method, which chooses at each iteration a correction image that not only minimizes χ^2 but is also orthogonal

to all previous corrections in the iterative procedure. They show that when combined with an appropriate scaling of the pixel values (called *iterative relaxation*), this *conjugate gradient* method produces a faster rate of convergence than a simple gradient, or steepest-descent, method. (In fact, it can be shown that the least-squares technique of Goitein (*15*), which damps the image correction matrix with a χ^2 minimizing scalar "step length," is identical to the steepest-descent relaxation method.)

Walters et al. (*10*) developed a "hybrid" iterative-analytic technique in which they convolution-filter and back-project the error projections at each iteration to correct the image. They avoid introducing interpolation errors into the reconstruction by directly calculating estimated projections without actually computing a new reconstructed image at each iteration. An empirically determined damping factor was used for each iteration. Chang (*11*) used a first-order postcorrection for attenuation in addition to filtering and back-projecting the error projections. This method improved the speed of convergence of the process, but it requires computing a new image before estimating projections. A step-length factor was not used to damp the correction matrix. These hybrid methods are faster than the gradient or conjugate-gradient methods.

Although most iterative techniques have demonstrated faithful reconstructions for a limited number of simulated and real phantoms, an absolute count compared with activity calibration curve for a real instrument, scanning arbitrary source and attenuating material distributions, has not yet been presented.

The iterative method we adopted for the multi-detector scanner is similar to the approach taken by Chang (*11*), with two important differences. First, the estimation of two-dimensional projection data from a hypothetical source distribution is more complicated for this scanner than for a rotating gamma camera that records one-dimensional projections along line-integrals. Second, a damping factor that minimizes χ^2 is calculated for each iteration to control convergence. This step-length factor is calculated by analogy to Goitein's (*15*) damping factor. However, the method is not equivalent to a steepest-descent relaxation method because each iteration's step *direction* is calculated by filtering and back-projecting the error projections and then correcting the error image to first order for attenuation, instead of by explicitly minimizing χ^2. It is presumed, but not assured, that such hybrid, iterative-analytic procedures will converge to a unique, minimum χ^2 solution. Full attenuation compensation is accomplished by the repeated application of a first-order correction.

The steps in the method are outlined below, and then described in more detail:

1. Obtain a starting image, $f^{(o)}(x,y)$, which is first-order corrected for attenuation.
2. Estimate two-dimensional projection data from the image, using the assumed or measured attenuation distribution for this transverse section.
3. Subtract each estimated projection from the corresponding real measured projection data to form *error projections*.
4. Reconstruct the error projections to form an *error image*, $\Delta^{(i)}(x,y)$, for the i'th iteration, which is also first-order corrected for attenuation.
5. Use the error image to calculate a damping factor, $\delta^{(i)}$, that minimizes χ^2.
6. Obtain the next image by calculating

$$f^{(i+1)}(x,y) = f^{(i)}(x,y) + \delta^{(i)}\Delta^{(i)}(x,y) \qquad (1)$$

for all pixels (x,y).

7. Then go to Step 2 and repeat until the estimated projection data match the real data within statistical errors (minimum χ^2).

The analytic reconstruction process used in Steps 1 and 4 to produce the starting image $f^{(o)}(x,y)$, as well as to obtain an error image from the error projections, is similar to the method described in the previous section. However, the first-order correction for attenuation is a multiplicative postcorrection to the filtered, back-projected image, instead of a precorrection to the raw data before filtering. This process may be written symbolically as:

$$A \sum_i R_{\theta_i}\left[\sum_{x'} P_i(x',y)*h(x-x')\right].$$

That is, we first convolve each tangential row of a projection (or error projection), P_i, with a one-dimensional filter, h. Then each two-dimensional filtered projection is rotated to angle θ_i and added to the other filtered, rotated projections. Finally, the attenuation postcorrection, A, is applied to the image. This array is calculated as follows:

$$A(x,y) = 1/\left[\frac{1}{M}\sum_{i=1}^{M} \exp\{-\mu\ell(x,y,\theta_i)\}\right], \qquad (2)$$

where ℓ is the distance from the image point (x,y) to the boundary of the attenuating material along a line perpendicular to the tangential scan direction of the detector at angle θ_i. μ is the measured or assumed attenuation factor. If a variable attenuation distribution, $\mu(x,y)$, is used, the exponential factor is integrated over the distribution along the lines $\ell(x,y,\theta_i)$.

Steps 1 and 4 could be replaced by any "black box" reconstruction, such as filtering the back-projection, without changing the basic algorithm for attenuation correction.

The estimation of the data (Step 2) measured by detector k when scanning the i'th iteration's hypothetical image is given by the following two-dimensional sum:

$$E_k^{(i)}(x,y) = \int\int f_k^{(i)}(x',y')\alpha_k(x,y,x',y') \times g_k(x-x',y-y')dx'dy', \qquad (3)$$

where $f_k^{(i)}(x',y')$ = image at i'th iteration rotated into detector k's coordinate system (See Fig. 1);
$\alpha_k(x,y,x',y')$ = the attenuation along a line from the image point (x',y') to the detector k when the detector's focal point is at (x,y);
$g_k(x - x', y - y')$ = the collimator's geometric line-source response; and
$E_k^{(i)}(x,y)$ = estimate of projection k data for the i'th iteration.

For the case of an ideal, attenuation-free medium, $\alpha = 1$ everywhere and Eq. 3 reduces to a simple two-dimensional convolution. This form has many computational advantages, but they do not hold for an attenuating object. This is because α is separately a function of the coordinates (x,y) and (x',y'), and not simply a function of the difference coordinates $(x - x', y - y')$.

However, we make the following approximation:

$$\alpha_k(x,y,x',y') \approx \alpha_k(x',y') \qquad (4)$$

= attenuation along a line (from the image point (x',y') to the object boundary) that is perpendicular to the scan direction of detector k.

Consider one term in the two-dimensional sum in Eq. 3, which is represented in Fig. 1. The true attenuation from (x',y') to Detector k when it is focussed at (x,y) is calculated from the line integral of the attenuation values along line d. Approximation 4 means using the line integral of the attenuation values along $d^{\perp}$ to calculate α for this term in the double sum. This is a good approximation because when (x',y') is far from the detector's central axis, the collimator's geometric response, g, becomes small. These terms therefore contribute little to the sum. Furthermore, as (x',y') approaches the detector axis, then d approaches $d^{\perp}$. This approximation means

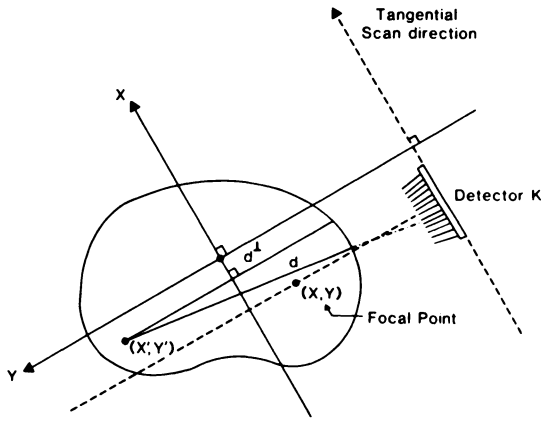

FIG. 1. Geometric approximation used to estimate projection data. True attenuation factor for one term in the two-dimensional sum in Eq. 3 (see text) is represented by the line integral of attenuation values along line d to patient boundary. Approximation 4 means using the line integral along line $d^{\perp}$ to calculate this term.

that a projection may be estimated simply by multiplying the hypothesized image by a precalculated attenuation grid for this projection and then convolving with the two-dimensional collimator response.

To test this approximation, we tried to see how closely we could match data estimated from a 20-cm cylindrical "flood" phantom of Tc-99m with real, measured data from such a phantom. Equation 3 was used with Approximation 4 to estimate the projections. The function, f(x,y), was assumed to be a centered, circular disk of uniform activity concentration. We varied the normalization of this distribution until the χ^2 function was minimized. The minimum χ^2 divided by the number of data points in a projection was 1.3. In addition to Approximation 4, there are other factors that could give $\chi^2 > 1.0$. For example, each collimator has a geometric line-source response that is slightly different from the others, due to the collimator fabrication technique. We used a Monte Carlo program to simulate the two-dimensional line-source response that is then used for the calculation of each estimated projection.

After the error image has been calculated, a damping factor, $\delta^{(i)}$, is calculated (Step 5), which should minimize the following function on the next iteration:

$$\chi^2 = \sum_k \sum_x \sum_y \frac{[P_k(x,y) - E_k^{(i+1)}(x,y)]^2}{[\sigma_k(x,y)]^2}, \qquad (5)$$

where $P_k(x,y)$ = measured projection data for detector k, and $\sigma_k(x,y)$ = random error at point (x,y).

The estimate of the next iteration's projection data, $E_k^{(i+1)}(x,y)$, is a function of $\delta^{(i)}$ and this iteration's image, $f^{(i)}(x,y)$, as follows:

$$E_k^{(i+1)}(x,y) = \sum_{x'} \sum_{y'} [f^{(i)}(x',y') + \delta^{(i)}\Delta^{(i)}(x',y')] \times \alpha_k(x',y')g_k(x - x', y - y') \qquad (6)$$

The χ^2 minimum condition,

$$\frac{\partial \chi^2}{\partial \delta^{(i)}} = 0 \qquad (7)$$

leads to the following value for the damping factor:

$$\delta^{(i)} = \frac{\sum_k \sum_x \sum_y [P_k(x,y) - E_k^{(i)}(x,y)]H_k^{(i)}(x,y)/[\sigma_k(x,y)]^2}{\sum_k \sum_x \sum_y [H_k^{(i)}(x,y)/\sigma_k(x,y)]^2}, \qquad (8)$$

where

$$H_k^{(i)}(x,y) = \sum_{x'} \sum_{y'} \Delta^{(i)}(x',y')\,\alpha_k(x',y')g_k(x - x', y - y'). \qquad (9)$$

The damping factor helps to control convergence of the reconstruction process and prevents overcorrection of the image, which could lead to oscillatory behavior.

For the iterative attenuation correction, the 128 × 22

measured projections were "double-binned" in the tangential scan direction to form 64 × 22 element arrays. The reconstructed image is 64 × 64. This is in contrast to the former reconstruction with a first-order multiplicative precorrection for attenuation, which used 128 × 22 projections and produced a 128 × 128 reconstructed image. Working with 64 × 22 arrays saves considerable computer time. The linear pixel size is 0.8 cm for a 64-element tangential scan line. This is half the full-width at half-maximum (FWHM) of the collimator line-source response at the focal point.

The convolution filter coefficients used during each iteration on each 64-element tangential scan row are shown in Table 1. We used the Fourier transform of a Blackman-windowed linear ramp. These coefficients, unlike those for the 128-element, first-order reconstruction, were not empirically optimized to produce a minimum deviation between a "known" distribution and the reconstructed image.

PERFORMANCE

The iterative attenuation correction has been tested with several physical phantoms of different sizes and shapes, and with varying distributions of radionuclide concentration. The reconstructions have also been compared with the simple first-order multiplicative precorrection described earlier.

TABLE 1. CONVOLUTION FILTER COEFFICIENTS USED FOR BOTH RECONSTRUCTIONS

128 × 128 First-order precorrection	64 × 64 Iterative blackman-windowed linear ramp
1.000	1.000
0.987	
0.518	0.683
0.009	
−0.449	0.062
−0.443	
−0.274	−0.310
−0.115	
−0.072	−0.297
−0.064	
−0.057	−0.155
−0.059	
−0.057	−0.082
−0.047	
−0.047	−0.063
−0.043	
−0.038	−0.045
−0.029	
−0.027	−0.031
−0.023	
−0.017	−0.028
−0.008	
−0.008	−0.023
−0.008	
−0.007	−0.018
−0.007	
	−0.015

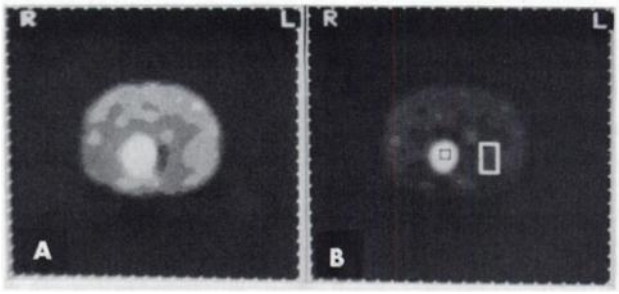

FIG. 2. Reconstructions of water-filled torso phantom containing 5-cm spherical flask with 6.0 times surrounding Tc-99m concentration. Also shown are rectangular regions of interest used to calculate average reconstructed concentrations. (A) With a simple, first-order precorrection for attenuation, indicated flask-to-background concentration ratio is 4.5. (B) After three iterations through our attenuation program, the ratio is 6.0.

In order to measure the approximate fraction of scattered photons present in our data, we first reconstructed an image of a water-filled, 5-cm-diameter cylinder containing no activity inside a 35-cm-diameter cylindrical phantom containing a uniform concentration of Tc-99m. With both the first-order and iterative attenuation corrections, the reconstructed average number of counts in the small cylinder was ~9% of the average number of counts in the large cylinder. When a water-filled, 5-cm-diameter spherical flask was used inside a torso-shaped phantom with uniform Tc-99m concentration, both reconstruction methods yielded a scatter fraction ~18%. (More scattering would be expected from a spherical region of no activity than from a cylindrical region, since photons can better penetrate the sphere from 4π solid angle before scattering.) Both measured scatter fractions disagree with the 40% scatter fraction used by Jaszczak, et al. (*17*). There are two possible explanations for this discrepancy. First, a sphere diameter of roughly twice our system's resolution was used. A larger scatter fraction would be measured inside a sphere with a size more consistent with the smaller resolution for a rotating gamma camera system. Second, the energy resolution of the scanning, multi-detector system is ~22% for Tc-99m. The energy window of the pulse-height analyzer was set asymmetrically around the photopeak from 130–170 keV, a setting chosen to optimize signal-to-noise ratio (*1*). The measured scatter fractions have been used to correct all further experimental data reported here (*17*).

Shown in Fig. 2 are reconstructions of a water-filled torso phantom containing a 5-cm-diameter spherical flask of higher Tc-99m concentration. This scan passes approximately through the middle of the flask. Fig. 2A is the first-order multiplicative correction reconstruction and Fig. 2B is the image after three iterations through

the attenuation-correction program. A water-filled ellipse with axes 28 and 23 cm was used to calculate the attenuation grids. (These dimensions were measured directly from the phantom using calipers.) The sphere-to-background ratio for the injected Tc-99m concentration was 6.0. Figure 2B also shows the two rectangular regions used to calculate average counts per pixel in the flask and in the background for both images. After scatter correction, the first-order correction gives the ratio 4.5, whereas iteratively correcting for attenuation yields 6.0. Although the regions used give the correct ratio for the iterative program, it can be seen that the indicated activity concentration systematically decreases from the front of the torso to the back. The display used to produce these photographs uses only 16 distinct gray levels. This can lead to gray-scale quantization effects that often cause the image to look artifactual. In Fig. 2B, the difference in average counts between regions in the front of the torso and the back was only 3.2% of the average count in the flask. This systematic difference in the background concentration leads to a spread of measured sphere-to-background ratios from 5.6 (7% low) to 6.6 (10% high). This may be due to approximation of the torso shape with that of an ellipse of water for attenuation compensation. Nevertheless, this error is comparable to the magnitude of the random noise in the background (~10%). The region of decreased activity immediately above the flask in Fig. 2B corresponds to the position of a small rubber stopper used to seal the flask.

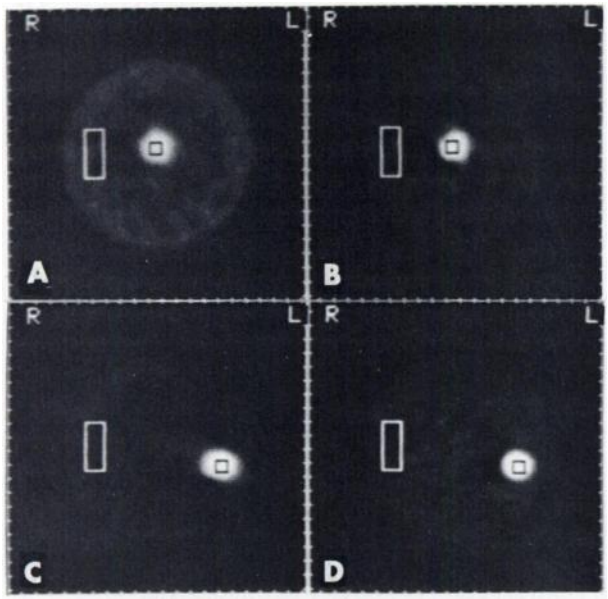

FIG. 3. Reconstructions of 35-cm diameter cylindrical phantom containing a single 5-cm vial with 10.3 times surrounding Tc-99m concentration. Also shown are rectangular regions of interest used to calculate average reconstructed concentrations. (A) When vial was centered in phantom, first-order precorrection gave vial-to-background concentration ratio of 4.6. (B) Three iterations through the attenuation program produced a ratio of 11.2. (C) When vial was near the edge, first-order correction gave a ratio of 12.0. (D) Three iterations through the attenuation program produced a ratio of 11.3.

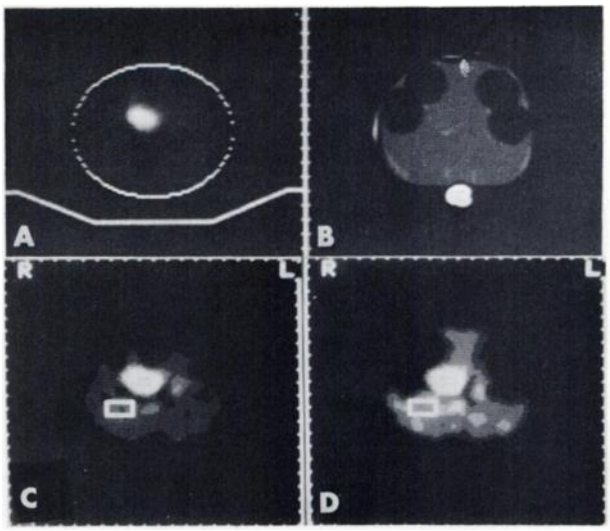

FIG. 4. Attenuation correction results using an ellipse-of-water approximation for attenuating material, compared with results using a "true" transmission CT image for attenuation compensation. Human torso phantom with 0.37 μCi/ml Tc-99m and external aluminum "bones" contains four air-filled balloons to simulate lungs. Plastic "organ" with 5.4 times surrounding Tc-99m concentration was inserted roughly in center of phantom. (A) Shows ellipse used to calculate attenuation grids, superimposed on first-order-corrected ECT image. Plexiglas patient couch under torso phantom is also included in calculation of attenuation grids. (B) Transmission CT image of this slice. (C) ECT image resulting from ellipse-of-water approximation in A. Indicated vial-to-background concentration ratio here is 10.1. (Image is enhanced to bring out background.) (D) ECT image resulting from TCT image in B. Indicated vial-to-background concentration ratio is 5.5.

Figure 3 shows reconstructions of a 35-cm-diameter cylindrical water phantom containing a single 5-cm-diameter vial of a higher activity concentration. The actual ratio of vial-to-background Tc-99m concentration was 10.3. Using the rectangular regions of interest shown, the first-order attenuation correction gives a ratio of 4.6 when the vial was centered (Fig. 3A) and 12.0 with the vial near the edge (Fig. 3C). Also, the first-order correction seriously distorts the shape of the distribution when the vial is off-center. By contrast, after three iterations through the attenuation program, the measured ratios are 11.2 (Fig. 3B) and 11.3 (Fig. 3D), respectively.

Although the assumption of a water-filled ellipse may work well for some attenuation and radionuclide distributions, for others it may be important to use a more accurate attenuation map. The human torso phantom with external aluminum "bones" was filled with a Tc-99m concentration of 0.37 μCi/ml. Four air-filled balloons were placed inside the Plexiglas phantom to simulate lungs. In addition, an irregularly shaped plastic "organ" containing 5.4 times the adjacent Tc-99m concentration was placed roughly in the middle of the phantom. (In the slice of Fig. 4 the cross section of this organ is approximately elliptical, with axes ~5 and 7 cm.) Figure 4A shows the ellipse (28 cm × 23 cm) used

to calculate attenuation grids; it is superimposed on the first-order corrected image. (The Plexiglas patient couch under the torso phantom is also included in the calculation of attenuation grids.) Figure 4C shows the corrected emission image resulting from the ellipse-of-water approximation. This image has been enhanced to bring out the background. Figure 4B is a TCT image of the attenuation in the same slice, obtained from a different scanner. When this image is used to calculate attenuation grids for the iterative reconstruction, Fig. 4D is the resulting emission image. Using superimposed rectangular regions, the indicated ratio of the organ concentration to the background concentration is 5.5 using this more accurate attenuation distribution, whereas the ellipse-of-water approximation seems to overcorrect the center, producing a ratio of 10.1. The first-order precorrection method gives 9.1.

To study the noise properties of the iterative reconstruction, we used a centered 20-cm-diameter flood phantom filled with a Tc-99m concentration of 0.9 μCi/ml. In a 5-min scan of one slice of this phantom, 1.4 million events were recorded. A transverse section of this flood contains ~47 resolution elements (2.6 × 2.6 cm). The % rms standard deviation of the pixel counts inside the two large regions of interest (one centered, the other near the edge) was calculated for the simple first-order attenuation corrected image, and for the iterative reconstruction. For the first-order precorrection, the central region had 3.2% rms noise, compared with 2.3% near the edge. After convergence (three iterations), the iterative reconstruction had 7.4% noise in the center and 6.9% near the edge. The noise changed less than 0.1% with each iteration after the third.

To check the absolute quantitative capabilities of this method, we fitted the reconstructed average number of counts per pixel in these regions of interest in Tc-99m phantoms to a linear function of injected concentration. The data are shown in Fig. 5 along with the straight line resulting from the fit. The errors shown and used in the fit are the standard deviations of the reconstructed counts inside the regions of interest.

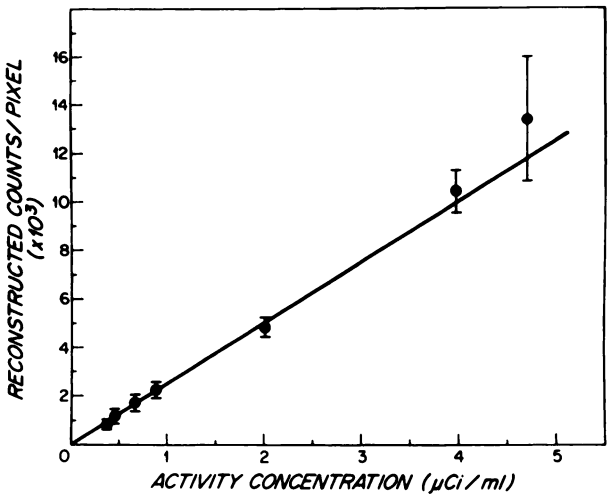

FIG. 5. System's absolute activity calibration curve for Tc-99m, obtained from phantoms of different size and source distributions after three iterations through attenuation program. Curve shown is straight-line fit to data. Errors are standard deviations of reconstructed counts inside regions of interest. Data points in increasing order of concentration are: (1) background in Fig 4D; (2) background in Fig. 3D; (3) background in Fig. 2B; (4) region in 20-cm flood used in noise determination; (5) "organ" in Fig. 4D; (6) spherical flask in Fig. 2B; (7) cylindrical vial in Fig. 3D.

DISCUSSION

The iterative attenuation correction leads to significantly better relative and absolute quantitative capabilities for this multi-detector emission tomographic scanner. The method converges in three iterations for most objects scanned. The assumption of an ellipse of water for attenuating material seems inadequate for scans that include bone and lungs in the same slice. This may limit the usefulness of analytic attenuation methods (*6–9*) that rely on the approximations of convex shape and uniform attenuation to invert the attenuated Radon transform. However, it is possible that an instrument with a different scan geometry would not be as sensitive to the "details" of the attenuating material. Clearly it is not practical to subject each patient to a TCT scan just to obtain an attenuation distribution with which to correct the emission tomographic image. However, it should be possible to develop a library of standard TCT attenuation maps through relevant human cross sections. An individual patient's major and minor elliptical axes could then be measured with calipers before the emission scan. The "standard-man" TCT image would then be "stretched" appropriately in the horizontal and vertical directions to be used for attenuation compensation. Such a procedure, of course, is not exact, but it should be much better than simply assuming an ellipse of uniform attenuation. We have not yet evaluated the possibility of using scattered radiation to indicate the approximate boundaries of highly attenuating regions.

We have also not evaluated activity measurement accuracy for objects of a size less than about twice the spatial resolution of the scanner. If this instrument is capable of providing accurate size and volume measurements, however, it should be straightforward to correct activity measurements for the well-known effect of contrast degradation due to finite spatial resolution. Using a first-order attenuation technique with correction for scattering and contrast loss by spatial resolution, Jaszczak et al. (*17*) have reported good accuracy of volumetric and activity measurement for spheres of several sizes in a water-filled cylinder having one tenth of the activity concentration.

The % rms noise in the reconstruction of a 20-cm-diameter flood phantom is higher for the iterative at-

tenuation correction than for the first-order correction. This is probably because the error projections at each step of the iterative procedure still contain noise, which is amplified by the convolution kernel shown in Table 1. Since the error image in the first few iterations is composed mainly of low spatial frequencies due to attenuation, it may be possible to use a smoother (low-pass) convolution filter to restore these frequencies without amplifying random noise as much. We have not yet evaluated other possible filters. Unlike the first-order correction method and analytic methods (*6,8*) used for other scan geometries, the image noise after convergence with this method seems fairly uniformly distributed over the reconstructed image.

Although this work provides a demonstration of absolute activity quantitation capabilities for a real instrument scanning a variety of distributions of source and attenuating material, all of the iterative methods mentioned in the section on Theory are, in principle, capable of the same. The main differences between the methods are the reconstruction time per iteration, the number of iterations required to converge, and the way noise is handled by the reconstruction. The gradient and conjugate methods (*5,16*) with weighted attenuation factors are purely iterative and do not use the analytic filtering and back-projection of error projections to correct the image at each iteration. They are therefore slower than the hybrid methods.

The hybrid method described by Walters et al. (*10*) reduces sampling artifacts by calculating estimated projections without the intermediate step of computing a new reconstructed image at each iteration. This procedure avoids introducing interpolation errors into the reconstruction process. However, these authors did not use a first-order attenuation correction to produce the starting image or to correct the error image at each iteration. Consequently their technique requires more iterations to converge than does Chang's method (*11*) or the method described here. Even though our reconstruction does use interpolation, it converges rapidly and adds less than 0.1% rms noise after the third iteration, for each iteration to a 20-cm flood.

Chang (*11*) used a first-order correction for attenuation at each step of his iterative reconstruction, but the error image was not added to the previous image with a multiplicative damping factor that minimizes χ^2. Also, there was no test for the consistency of estimated and real projection data. We have found that the calculated damping factor is important and can vary from 0.2 to 1.0, depending on the iteration number, the size of the object, and the distributions of source and attenuating material. When δ is set equal to 1.0 for each iteration, the iterative procedure for this multi-detector scanner may take many more iterations to converge, if it converges at all.

With a Data General Eclipse 230 minicomputer, the previous, first-order reconstruction time was 2 min per slice. The iterative program currently requires 3 min per iteration. (Calculation of new attention grids requires 8 min.) Both of these times could be significantly reduced by using an array processor.

FOOTNOTES

‡ Cleon Imager, Union Carbide.

§ The filter coefficients were iteratively varied to produce an optimal, least-squares reconstruction of a cylindrical phantom containing three separate concentric regions of different activity concentrations. The inner circle and the outer annulus had the same concentrations and the middle annulus contained no radioactivity.

REFERENCES

1. KIRSCH CM, MOORE SC, ZIMMERMAN RE, et al: Characteristics of a scanning, multi-detector, single-photon ECT body imager. *J Nucl Med* 22:726-731, 1981
2. KUHL DE, EDWARDS RQ, RICCI AR, et al: Quantitative section scanning using orthogonal tangent correction. *J Nucl Med* 14:196-200, 1973
3. KAY DB, KEYES JW, JR: First order corrections for absorption and resolution compensation in radionuclide Fourier tomography. *J Nucl Med* 16:540-541, 1975 (abst)
4. KUHL DE, EDWARDS RQ, RICCI AR, et al: The Mark IV system for radionuclide computed tomography of the brain. *Radiology* 121:405-413, 1976
5. BUDINGER TF, GULLBERG GT: Transverse section reconstruction of gamma-ray emitting radionuclides in patients. In *Reconstruction Tomography in Diagnostic Radiology and Nuclear Medicine.* M. M. Ter-Pergossian et al., Eds. Baltimore, University Park Press, 1977, pp 315-342
6. TRETIAK OJ, DELANEY P: The exponential convolution algorithm for emission computed axial tomography. In *Review of Information Processing in Medical Imaging*, Brill AB, Price RR, Eds. Oak Ridge National Laboratory Report ORNL/BCTIC-2, 1978, pp 266-278
7. GULLBERG GT: The attenuated Radon transform: theory and application in medicine and biology. Ph.D. Thesis, Lawrence Berkeley Laboratory, University of California, 1979, pp 211-242
8. GULLBERG GT, BUDINGER TF: The use of filtering methods to compensate for constant attenuation in single-photon emission computed tomography. *IEEE Trans Biomed Eng* BME-28:142-157, 1981
9. BELLINI S, PIACENTINI M, CAFFORIO C, et al: Compensation of tissue absorption in emission tomography. *IEEE Trans Acoustics, Speech and Signal Processing* ASSP-27: 213-218, 1979
10. WALTERS TE, SIMON W, CHESLER DA, et al: Attenuation correction in gamma emission computed tomography. *J Comp Assist Tomogr* 5:89-94, 1981
11. CHANG LT: A method for attenuation correction in radionuclide computed tomography. *IEEE Trans Nucl Sci* NS-25:638-643, 1978
12. STODDART HF, STODDART HA: A new development in single gamma transaxial tomography: Union Carbide focussed collimator scanner. *IEEE Trans Nucl Sci* NS-26:2710-2712, 1979
13. ZIMMERMAN RE, KIRSCH CM, LOVETT R, et al: Single photon emission computed tomography with short focal length detectors. In *Single Photon Emission Computed Tomography and Other Selected Computer Topics.* Price RR, Gilday DL, Croft BY, Eds. New York, Society of Nuclear Medicine, 1980, pp 147-157

14. FLOWER MA, PARKER RP: Quantitative imaging using the Cleon emission tomography system. *Radiology* 137:535-539 1980
15. GOITEIN M: Three dimensional density reconstruction from a series of two-dimensional projections. *Nucl Instr Meth* 101:509-518, 1971
16. HUESMAN RH, GULLBERG GT, GREENBERG WL et al: RECLBL library user's manual—Donner algorithms for reconstruction tomography. Technical Report PUB 214. Lawrence Berkeley Laboratory, 1977
17. JASZCZAK RJ, COLEMAN RE, WHITEHEAD FR: Physical factors affecting quantitative measurements using camera-based single photon emission computed tomography (SPECT). *IEEE Trans Nucl Sci* NS 28:69-80, 1981

New England Chapter Annual Meeting
Society of Nuclear Medicine

October 22-24, 1982 **Sheraton-Islander Inn** **Newport, Rhode Island**

The New England Chapter's Annual Meeting is geared to all general radiologists and nuclear medicine physicians, technologists, and other practitioners interested in nuclear medicine. An important refinement of cardiac imaging has been the development of practical means for quantification. These means will be discussed in detail the first day of the meeting. The evening will be devoted to an intensive review of practical and interesting clinical cases. The morning of the second day will be devoted to new procedures and techniques of practical importance in clinical nuclear medicine; the afternoon program will include special sessions for technologists. The fifth annual Blumgart Award ceremony will take place at the special mid-day banquet. Recipient this year is Dr. H. William Strauss, Dir. of Nuclear Medicine at Massachusetts General Hospital in Boston. Several medical centers in the United States have gained experience with the research and clinical capabilities of nuclear magnetic resonance. A symposium chaired by Dr. Thomas Brady of Massachusetts General Hospital will conclude this three-day meeting. Augmenting the formal instructions will be exhibits of technical equipment by a variety of manufacturers.

The distinguished faculty will include Drs. Charles Boucher, Thomas Brady, Louis Bravaman, Fernando Buounanno, John Clements, Leonard Holman, Bertram Pitt, Ian Pykatt, Peter Schneider, Richard Spencer, William Strauss, Franz Wackers, and Alan Waxman.

The program is approved for AMA Category I: 12 hr. Tuition is $60 for physicians who are members of the Society of Nuclear Medicine; $125 for nonmember physicians; $35 for technologists. Tuition will include dinner, lunch, and refreshments at breaks.

For further information contact:

Educational Resources Associates, Inc.
P.O. Box 369
Brookline, MA 02146
Tel: (617)738-8859 or 8861